2024 IEEE International Conference on Robotics and Automation (ICRA 2024)
May 13-17, 2024. Yokohama, Japan

Modeling and Control of PADUAV: a Passively Articulated Dual UAVs Platform for Aerial Manipulation*

Jiali Sun[1], Kaidi Wang[1], Chuanbeibei Shi[1], Xiujia Li[1], Xiaojian Yi[1], Yushu Yu[1], Fuchun Sun[2], Yiqun Dong[3]

***Abstract*— In this paper, we introduce PADUAV, a novel 5-DOF aerial platform designed to overcome the limitations of traditional tiltrotor vehicles. PADUAV features a unique mechanical design that incorporates two off-the-shelf quadrotors passively articulated to a rigid frame. This innovation enables free pitch rotation without mechanical constraints like cable winding, significantly enhancing its capabilities for various tasks. To control PADUAV's 5 degrees of freedom, we propose a versatile and straightforward 5-DOF geometric tracking control strategy that generates 2D force and 3D torque. A decomposition approach is designed to distribute the output to the torque and thrust commands for each subplane, with no need for complex optimization. We validate our approach through three simulation experiments conducted in the Gazebo environment, leveraging the utilities provided by the RotorS simulator. These experiments not only demonstrate the feasibility of our platform but also provide new perspectives for future aerial platform development, particularly in terms of simulation-based approaches.**

I. INTRODUCTION

With the rapid development of unmanned aerial vehicles (UAVs), researchers are no longer confined to investigating perceptual functions such as surveillance and SLAM (Simultaneous Localization and Mapping). The vast potential of aerial task dealing is being actively explored [1]–[7]. Examples include aerial additive manufacturing robots capable of 3D printing in midair [8] and the M4 multimodal robot that transforms its wheels into thrusters to perform high-altitude rescue [9].

In recent years, an array of novel platforms has emerged within the field of aerial robotics. To perform aerial grasping tasks, some platforms are designed with large shapes to accommodate the weight of manipulators [10]. Others integrate multiple UAVs to execute cable-suspended aerial transportation missions [11]–[13]. Aerial tasks encompass far more than mere grasping and transport [14], [15]. It is increasingly likely that aerial robots will supplant humans in performing intricate operations within inaccessible, irregular, or hazardous environments. Such demands underscore the need for platform flexibility. To overcome the movement limitations of traditional UAVs, the addition of actuators is often considered to create more flexible 5- and 6-DOF platforms, which are more capable of performing aerial manipulation tasks [16]–[21]. In the review [22], aerial manipulation is categorized into four workspaces based on tool placement: underside, upperside, lateral side, and further down side.

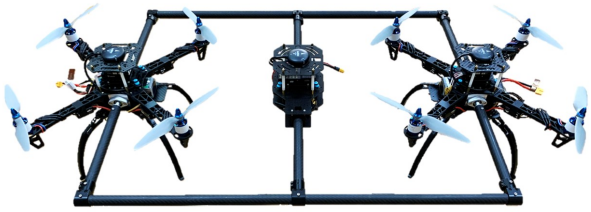

Fig. 1. Prototype of the proposed PADUAV platform.

However, with 5- and 6-DOF platforms, this problem could become platform-oriented so that the installation place of the tools does not matter in finding the workspace. This work aims to enlarge the aerial manipulation scope by addressing common challenges encountered by tilting aerial platforms. The primary challenge lies in the mechanical domain. Despite the 6-DOF capabilities of Voliro [23], enabled by servo motors that support 720° rotor rotation, limitations arise due to the winding of thrust motor cables around the arms, restricting rotation to specific angular positions. This limitation is not unique to Voliro but is shared by other aerial vehicles employing servo motors for tilting, such as [24]–[26]. Additionally, tilted drones with fixed rotors, like the cube-like vehicle in [27] and Odar in [28], achieve 6-DOF but face the challenge of rotor reversing as they pass through singular postures. This necessitates the development of complex algorithms to mitigate the adverse effects of rotor reversing, posing engineering difficulties. Modular quadrotor platforms like SmQ and S2Q utilize two or three quadrotors connected to the platform via ball joints, offering simpler designs [29], [30]. However, their rotational motion remains confined to a limited range. The over-actuated multi-rotor aerial vehicle proposed by Tsao et al. is able to complete 360° rotation [31]–[33]. However, as an over-actuated platform, their proposed gimbal structure remains complex, and their work does not include an analysis of quadrotor dynamics.

In light of these limitations, we introduce PADUAV, a 5-DOF platform actuated by two quadrotors that are passively articulated to a rigid frame. This platform can perform independent movements in five directions, including translation in three directions and rotation in two directions. The contributions of this work are summarized as follows:

- The designed PADUAV successfully overcomes the

*This work was supported by the National Natural Science Foundation of China under Grant 62173037. (Corresponding author: *Yushu Yu.*)

[1]School of Mechatronical Engineering, Beijing Institute of Technology, Beijing 100081, China yushu.yu@bit.edu.cn

[2]Department of Computer Science and Technology, Tsinghua University, Beijing 100084, China fcsun@mail.tsinghua.edu.cn

[3]Department of Aeronautics and Astronautics, Fudan University, Shanghai 200433, China yiqundong@fudan.edu.cn

cable winding issue that limits free pitch rotation. additionally, it has a simpler structure, can be actuated by a five-dimensional wrench, and is capable of full rotation without additional actuators. To the best of our knowledge, this makes it the first aerial platform with all these features.

- Unlike previous research, the closed-form system dynamics is established taking into account the quadrotor dynamics. The dynamics are further decoupled for the purpose of control design. Our proposed control framework includes a modified geometric controller and an output decomposition approach, offering a simple yet versatile method for generating 5-DOF control outputs.
- Three Gazebo-based simulation experiments, utilizing the plugins provided by RotorS, are conducted, representing a noteworthy contribution in the field of visually-assisted controller design and tuning for novel aerial platforms.

II. Mechanical Design and Modeling

A. Mechanical Design

The proposed PADUAV is a platform actuated by two off-the-shelf quadrotors, which will be referred to as 'subplanes' in subsequent sections. These subplanes are passively articulated to a rigid frame composed of transverse and longitudinal carbon fiber tubes connected by six T-shaped tube clamps. At the geometric center of the platform, a stack of carbon fiber disks, referred to as the center, accommodates the onboard computer, flight controller, GPS, battery, and any necessary operation tools.

As shown in Fig. 2, two bearing seats are designed to form the revolute joints that enable the subplanes to rotate around the side longitudinal tubes. A notable distinction between our tilting platform and others is our utilization of complete quadrotors, which possess intrinsic torque and thrust generation capabilities to achieve tilting, unlike platforms relying on servos to drive rotors.

Note that the two subplanes and the center stack receive power independently, and there are no power wires connecting the center and the subplanes. As long as the communication between the subplane flight controller and the onboard computer is wireless, there will be no wiring issue limiting the tilting angle as encountered in [24], [26]. This is technically feasible in that previously mentioned works have implemented reliable wireless communication between the host computer and multiple UAVs, for example, [30] uses XBee communication and [11] uses Wi-Fi communication.

B. Dynamics Modeling

The coordinate system is established as shown in Fig. 2. The Earth frame $\{E\}$ follows the East-North-Up (ENU) convention, while the body frame $\{B\}$ is fixed at the center of the main body. The subplane body frames are labeled as $\{S_1\}$ and $\{S_2\}$. For each subplane ($i = 1, 2$), $F_i \in \mathbb{R}^3$ represents thrust and $\tau_i \in \mathbb{R}^3$ denotes torque. In the S_i frames, there are ${}^{S_i}F_i = [0, 0, F_{iz}]^T$ and ${}^{S_i}\tau_i = [\tau_{ix}, \tau_{iy}, \tau_{iz}]^T$. Throughout the paper, subscript i will be used to refer to the subplane for brevity. Also, the coordinate systems will not be explicitly specified when performing vector operations.

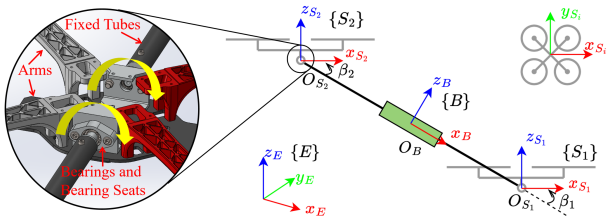

Fig. 2. Cross-sectional diagram of the platform for a better illustration of its mechanical characteristics. The earth, body, and subplane coordinate systems are defined. The enlarged view of the articulation joint is given in the left CAD model. Two pairs of bearings are installed at the sides of a subplane so that it can rotate relatively to the fixed tubes.

The system motion is composed of three parts, namely the translation of the system center of mass(COM), the rotation of the system's main body, and the axial rotation of the subplanes relative to the main body.

Let ${}^E p_b = [x, y, z]^{\mathrm{T}} \in \mathbb{R}^3$ denote the main body position expressed in $\{E\}$. The main body attitude is represented by $R_b \in \mathrm{SO}(3)$. Given that the entire system resembles a floating-base manipulator, with each subplane acting as a link, we introduce $r = [\beta_1, \beta_2]^{\mathrm{T}} \in \mathbb{R}^2$ as the joint angles between the subplane and the main body. This choice simplifies the derivation of dynamic equations using the Newton-Euler approach. Consequently, the configuration of the system can be expressed as $H = ({}^E p_b, R_b, r) \in \mathbb{R}^3 \times \mathrm{SO}(3) \times \mathbb{R}^2$. The system's velocity is given by $\zeta = [{}^B v_b; {}^B \omega_b; \dot{r}] \in \mathbb{R}^6 \times \mathbb{R}^2$, where $[{}^B v_b; {}^B \omega_b]$ represents the body velocity of the middle platform. The selected system configuration variables correspond to the three sub-motions mentioned above.

The acceleration of the body frame origin O_B, a_b, consists of the tangential acceleration $\dot{v}_b$ and the normal acceleration $\omega_b \times v_b$ as given in (1). Then, forward iteration is performed to derive the subplane accelerations and angular velocities.

$$a_b = \dot{v}_b + \omega_b \times v_b \tag{1}$$

$$a_i = a_b + \dot{\omega}_b \times p_{ci} + \omega_b \times (\omega_b \times p_{ci}) \tag{2}$$

$$\omega_i = \omega_b + \dot{\beta}_i y_{S_i} \tag{3}$$

where $p_{ci} = \overrightarrow{O_B O_{Si}}$, y_{S_i} is the unit vector of frame $\{S_i\}$.

Assume the masses of subplane i and the main body are m_i and m_b, the inertia of the subplane is $J_i = \mathrm{diag}([J_{ixx}, J_{iyy}, J_{izz}])$, and that of the main body is J_b. Additionally, g represents gravitational acceleration. The joint torques and forces of the subplanes are given by:

$$n_i = J_i \dot{\omega}_i + \omega_i \times J_i \omega_i \tag{4}$$

$$f_i = m_i a_i - m_i g \tag{5}$$

Note that (4) also represents subplane dynamics. Due to the existence of revolute joints, there will be no torque interaction between the subplanes and the main body in their relative rotation. The torque components $n_{1y} y_{S_1}$ and $n_{2y} y_{S_2}$ will be removed when computing the body torque τ_b. The

backward iteration is given as:

$$F_b = m_b a_b - m_b g + f_1 + f_2 \tag{6}$$

$$\begin{aligned}\tau_b = {} & J_b\dot{\omega}_b + \omega_b \times (J_b\omega_b) + n_1 - n_{1y}y_{S_1} \\ & + n_2 - n_{2y}y_{S_2} + p_{c1} \times f_1 + p_{c2} \times f_2\end{aligned} \tag{7}$$

The system dynamics can thus be established as:

$$M(r)\dot{\zeta} + C(r,\zeta) + G(r,R_b) = {}^B\tau_e \tag{8}$$

Here, ${}^B\tau_e = [{}^BF_b; {}^B\tau_b; n_{1y}; n_{2y}] \in \mathbb{R}^8$, and $M(r) \in \mathbb{R}^{8\times8}$, $C(r,\zeta) \in \mathbb{R}^8$, and $G(r,R_b) \in \mathbb{R}^8$ are the mass matrix, centrifugal and Coriolis vector, and gravity vector. And τ_e is mapped from real inputs by force and torque equivalence:

$$\begin{aligned}F_b &= F_1 + F_2 \\ \tau_b &= \tau_1 + \tau_2 - \tau_{1y}y_{S_1} - \tau_{2y}y_{S_2} + p_{c1} \times F_1 + p_{c2} \times F_2 \\ n_{iy} &= \tau_{iy}\end{aligned} \tag{9}$$

Since the subplane thrusts F_1 and F_2 both lie in $\{xOz\}_B$ plane, there are ${}^BF_b = [{}^BF_{b,x}, 0, {}^BF_{b,z}]^T$ and ${}^B\tau_b = [{}^B\tau_{b,x}, {}^B\tau_{b,y}, {}^B\tau_{b,z}]^T$, indicating that the platform has five degrees of freedom.

C. Dynamics Decoupling

As previously mentioned, the system motion is composed of three sub-motions. It is natural that we want to design three controllers for each sub-motion. To eliminate the complicated loop interactions between the controllers, it is necessary to decouple them so that a change in one process variable will not cause corresponding changes in other process variables. Since the subsequent controller design will be model-based, the current dynamics should be decoupled into three sets of independent equations. For a specific sub-motion, the expected decoupled dynamics will exclude variables irrelevant to it.

1) Decouple the Translation Motion from General Rotations: Define the dynamics responsible for translation motion as "locked system" and the dynamics responsible for general rotations as "shape system", their equivalent inputs are τ_L and τ_E respectively. The COM position and velocity are denoted as p_L and v_L. By adopting the approach proposed in [34], the system dynamics in (8) can be decoupled as:

$$\text{locked system} \begin{cases} {}^E\dot{p}_L = {}^Ev_L \\ m_L{}^E\dot{v}_L - m_L{}^Eg = {}^E\tau_L \end{cases} \tag{10}$$

$$\text{shape system} \begin{cases} \dot{\sigma} = \sigma\hat{\mu} \\ M_E(r)\dot{\mu} + C_E(r,\mu) = {}^B\tau_E \end{cases} \tag{11}$$

where $m_L := m_b + m_1 + m_2 > 0$ is the total mass, ${}^Eg = [0,0,-9.81]^T$, $\mu = [{}^B\omega_b; \dot{r}]$, $\sigma = (R_b, r) \in \mathrm{SO}(3) \times \mathbb{R}^2$ and $\sigma\hat{\mu} = (R_b^{\mathrm{T}}\hat{{}^B\omega_b}, \dot{r})$. In the shape system, $M_E(r) \in \mathbb{R}^{5\times5}, C_E(r,\mu) \in \mathbb{R}^5$ are the mass matrix, centrifugal and Coriolis vector.

It can be found that there are no translation-related variables like linear velocities in the shape system dynamics, and no rotation-related variables like angular velocities in the locked system dynamics either, which means the first stage decoupling is finished.

In fact, by observing the internal structure of the dynamics (8), we find that if the masses of the subplanes are equal and the distances of their COMs to the center are equal, then the first three rows of (8) will be equivalent to the locked system dynamics (10) and the last five rows will be equivalent to the shape system dynamics (11). This indicates that the proposed mechanical design will lead to intrinsic decoupled features of the two types of motion under ideal circumstances.

2) Decouple the Main Body Rotation and Subplane Axial Rotation: From (3), we have:

$${}^{S_i}\dot{\omega}_{iy} = {}^{S_i}\dot{\omega}_{by} + \ddot{\beta}_i \tag{12}$$

Let $\lambda = [{}^{S_1}\omega_{1y}, {}^{S_2}\omega_{2y}]^T$, and then the term $M_E(r)\dot{\mu}$ in the shape system dynamics can be rewritten as follows:

$$\begin{aligned}M_E(r)\dot{\mu} &= \begin{bmatrix} M_{Er}(r){}^B\dot{\omega}_b \\ J_{1yy}({}^{S_1}\dot{\omega}_{by} + \ddot{\beta}_1) \\ J_{2yy}({}^{S_2}\dot{\omega}_{by} + \ddot{\beta}_2) \end{bmatrix} = \begin{bmatrix} M_{Er}(r){}^B\dot{\omega}_b \\ J_{1yy}{}^{S_1}\dot{\omega}_{1y} \\ J_{2yy}{}^{S_2}\dot{\omega}_{2y} \end{bmatrix} \\ &= \underbrace{\begin{bmatrix} M_{Er}(r) & \boldsymbol{O}_{3\times2} \\ \boldsymbol{O}_{2\times3} & M_{yy} \end{bmatrix}}_{:=M'_E(r)} \begin{bmatrix} \dot{\omega}_b \\ \dot{\lambda} \end{bmatrix}\end{aligned} \tag{13}$$

where $M_{Er}(r) \in \mathbb{R}^{3\times3}$, $M_{yy} = \mathrm{diag}(J_{1yy}, J_{2yy})$. $M'_E(r)$ and $C_E(r,\mu)$ possess the following structures:

$$\begin{aligned}M'_E(r) = {} & \begin{bmatrix} M_{res} & \boldsymbol{O}_{3\times2} \\ \boldsymbol{O}_{2\times3} & M_{yy} \end{bmatrix} \\ & + \Sigma_{i=1}^2(J_{ixx} - J_{izz}) \begin{bmatrix} M_{ixz}(\beta_i) & \boldsymbol{O}_{3\times2} \\ \boldsymbol{O}_{2\times3} & \boldsymbol{O}_{2\times2} \end{bmatrix}\end{aligned} \tag{14}$$

$$\begin{aligned}C_E(r,\mu) &= C_E(r, {}^B\omega_b, \dot{r}) \\ &= \begin{bmatrix} C_{res}({}^B\omega_b) \\ \boldsymbol{O}_{2\times1} \end{bmatrix} + \Sigma_{i=1}^2 J_{iyy}C_{iy}(\beta_i, \dot{\beta}_i, {}^B\omega_b) \\ &\quad + \Sigma_{i=1}^2(J_{ixx} - J_{izz})C_{ixz}(\beta_i, \dot{\beta}_i, {}^B\omega_b)\end{aligned} \tag{15}$$

The subscript $_{res}$ implies the meaning of residue, which is used to indicate the remaining term after decoupling as shown later.

It is seen that if $||J_{ixx} - J_{izz}|| = 0$ and $J_{iyy} = 0$, then the $\dot{\omega}_b$-dynamics and $\dot{\lambda}$-dynamics are completely decoupled from each other. In this case, rewriting ${}^B\tau_E = [{}^B\tau_{E,res}; {}^B\tau_{E,yy}] \in \mathbb{R}^3 \times \mathbb{R}^2$, the decoupled $\dot{\omega}_b$-dynamics and $\dot{\lambda}$-dynamics is summarized as follows:

$$\begin{aligned}M_{res}{}^B\dot{\omega}_b + C_{res}({}^B\omega_b) &= {}^B\tau_{E,res} \\ M_{yy}\dot{\lambda} &= {}^B\tau_{E,yy}\end{aligned} \tag{16}$$

The actual system may not satisfy the condition $||J_{ixx} - J_{izz}|| = 0$ and $J_{iyy} = 0$. However, with small $||J_{ixx} - J_{izz}||$ and J_{iyy}, the actual system can be regarded as a perturbed system expressed by (16).

III. Controller Design

In this section, we'll establish three sub-controllers based on the decoupled dynamics outlined in Section II-C. These sub-controllers will be linked together using intermediary modules to create the overall controller, enabling stable tracking of motion in the x, y, z, yaw, and pitch directions for our PADUAV platform. Refer to Fig. 3 for an illustration of the control process.

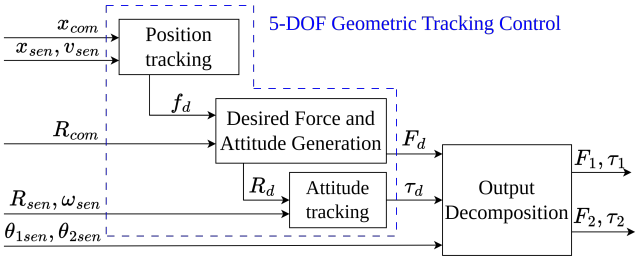

Fig. 3. Schematic diagram of the proposed control framework. It consists of a general 5-DOF geometric tracking control stage and a specific output decomposition stage.

A. 5-DOF Geometric Tracking Control

To enable 6-DOF maneuverability, we propose a 5-DOF geometric tracking control strategy based on the classic geometric tracking controller [35]. It consists of two cascaded sub-controller modules to achieve independent tracking of the translational motion and rotational motion. An additional module that generates the desired force and attitude is introduced to address the underactuation property of the platform. We stress the number of DOFs to show that this module group produces a 5-DOF output.

1) Position and Attitude Control: We define the following tracking errors: $e_x = x_{sen} - x_{com}$, $e_v = v_{sen} - \dot{x}_{com}$, $e_R = \frac{1}{2}(R_d^{\mathrm{T}} R_{sen} - R_{sen}^{\mathrm{T}} R_d)^{\vee}$, $e_\omega = \omega_{sen} - R_{sen}^{\mathrm{T}} R_d \omega_d$, where subscript $_{sen}$ and denotes sensor values, subscript $_{com}$ denotes the external command, and subscript $_d$ denotes the internal desired value passed from the upstream module.

Based on the decoupled dynamics (10) and (16), the position and attitude tracking control laws are expressed as:

$$\begin{cases} {}^E f_d &= m(-k_x e_x - k_v e_v + \ddot{x}_{com} + g e_3) \\ {}^B \tau_d &= M_{res}(-k_R e_R - k_\omega e_\omega) + C_{res}(\omega_{sen}) \end{cases} \tag{17}$$

where k_x, k_v, k_R and k_ω are positive constant gains. The commanded force is expressed in the earth frame $\{E\}$. The desired torque is expressed in the body frame $\{B\}$.

2) Desired Attitude Generation: In Section III, ZXY Euler angles are introduced to describe the rotation characteristics of both the platform and the subplane. To distinguish these angles from the traditional ZYX convention, the superscript $'$ will be added to the ZXY Euler angles. Then, the main body attitude can be expressed as:

$$R_b = R_z(\psi_b')R_x(\phi_b')R_y(\theta_b') \tag{18}$$

The subplane attitude can be expressed as:

$$\begin{aligned} R_{si} &= R_b R_y(\beta_i) = R_z(\psi_b')R_x(\phi_b')R_y(\theta_b' + \beta_i) \\ &= R_z(\psi_b')R_x(\phi_b')R_y(\theta_i') \end{aligned} \tag{19}$$

It can be seen that the subplane and the main body share a common yaw(ψ_b') and roll(ϕ_b') rotation. We introduce an intermediate frame $\{M\}$ that locates its origin at O_B, and its attitude is given by $R_m = R_z(\psi_b')R_x(\phi_b')$. Note that plane $(xOz)_M$ and plane $(xOz)_B$ are the same.

Since the system can only generate force in plane $(xOz)_B$, the desired attitude should also include the desired force in its $(xOz)_B$ plane. The commanded attitude R_{com} can be decomposed as $R_{com} = R_z(\psi_{com})R_y(\theta_{com})$. Similar to the approach proposed in [35], we make the following definitions: $b_{1d} := R_z(\psi_{com})e_1$, $b_{2d} := \frac{{}^E f_d \times b_{1d}}{||{}^E f_d \times b_{1d}||}$, and $b_{3d} = b_{1d} \times b_{2d}$, then the desired attitudes for frame $\{M\}$ and frame $\{B\}$ will be expressed as:

$$R_{dm} = [b_{1d}, b_{2d}, b_{3d}], \quad R_d = R_{dm} R_y(\theta_{com}) \tag{20}$$

And ω_d can be obtained by $\hat{\omega}_d = R_d^{\mathrm{T}} \dot{R}_d$, where the symbol $\wedge$ denotes the 3d-vector-to-skew-matrix operation.

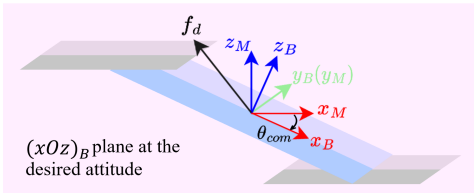

Fig. 4. Illustration of the introduced intermediate frame $\{M\}$ and its relation with $\{B\}$. The desired attitude should include the commanded force within its $(xOz)_B$ plane.

This guarantees that the desired force will lie in the plane $(xOz)_B$ of R_d. See Fig. 4. In frame $\{M\}$, the axial rotation of subplanes can be described by the pitch angle θ_i', while in frame $\{B\}$ the joint angle β_i is needed. However, joint angles are related to both main body pitch angle θ_b' and subplane pitch angle θ_i', which does not meet previous requirements of decoupling. Therefore, for the subsequent control of subplane axial rotation, the variable to be tracked is chosen as θ_i'. In addition, this angle also indicates the direction of the thrust that a subplane generates inside the plane $(xOz)_B$, thus it is reasonable to express the commanded force in frame $\{M\}$ as ${}^M F_d = [{}^M F_{d,x}; 0; {}^M F_{d,z}]$ so that it can be mapped to the real thrusts while the desired value of θ_i' can also be interpreted.

B. Output Decomposition

Let $u_e = [{}^M F_{d,x}, {}^M F_{d,z}, {}^B \tau_{d,x}, {}^B \tau_{d,y}, {}^B \tau_{d,z}]^T \in \mathbb{R}^5$, and this output of the 5-DOF geometric tracking control strategy should be decomposed to the real input $u_i = [F_{iz}, \tau_{ix}, \tau_{iy}, \tau_{iz}]^T \in \mathbb{R}^4$ for the subplane to execute. Note that if ϕ is small enough compared to θ and ψ, we have $R = R_z(\psi)R_y(\theta)R_x(\phi) \approx R_z(\psi)R_y(\theta) \approx R_z(\psi)R_x(0)R_y(\theta)$ then there are $\theta' \approx \theta$ and $\psi' \approx \psi$. Since the proposed platform is not intended for aggressive flight maneuvers, we can safely assume that $\theta_b' = \theta_b$ and $\theta_i' = \theta_i$.

1) Order Reduction Mapping: Define the intermediate value $\theta_d' := \mathrm{atan2}({}^M F_{d,x}, {}^M F_{d,z})$, which is the desired ZXY pitch angle for the two subplanes. By value binding, we let $\tau_{1x} = \tau_{2x} = \tau_{ix}$, $\tau_{1z} = \tau_{2z} = \tau_{iz}$. Similar to (9), the desired torque τ_{ix} and τ_{iz}, and the desired thrust F_{1z} and F_{2z} can be determined by solving the below equations:

$$\begin{bmatrix} {}^M F_{d,x} \\ {}^M F_{d,z} \\ {}^B \tau_{d,y} \end{bmatrix} = \begin{bmatrix} s\theta_d' & s\theta_d' \\ c\theta_d' & c\theta_d' \\ -c\beta_{1d} p_{c1} & c\beta_{2d} p_{c2} \end{bmatrix} \begin{bmatrix} F_{1z} \\ F_{2z} \end{bmatrix} \tag{21}$$

$$\begin{bmatrix} {}^B \tau_{d,x} \\ {}^B \tau_{d,z} \end{bmatrix} = \begin{bmatrix} (c\beta_{1d} + c\beta_{2d})/2 & (s\beta_{1d} + s\beta_{2d})/2 \\ -(s\beta_{1d} + s\beta_{2d})/2 & (c\beta_{1d} + c\beta_{2d})/2 \end{bmatrix} \begin{bmatrix} \tau_{ix} \\ \tau_{iz} \end{bmatrix}$$

where $\beta_{1d} = \beta_{2d} = \theta'_d - \theta'_b \approx \theta'_d - \theta_b$, and "c" and "s" are shorthand notations for cos and sin, respectively.

2) Subplane Axial Rotation Tracking: The values of τ_{1y} and τ_{2y} will be determined by introducing an axial rotation tracking controller, where θ'_d serves as the reference input. The justification of this design is explained in Section III-A.2. Tracking errors are given by: $e_{\theta'_i} = \theta'_i - \theta'_d \approx \theta_i - \theta'_d, e_{\dot{\theta}'_i} = \dot{\theta}'_i - \dot{\theta}'_d$, where $\dot{\theta}'_i = {}^{S_i}\omega_{iy}$. The control law is then given as:

$$\tau_{iy} = -k_{\theta'_i} e_{\theta'_i} - k_{\dot{\theta}'_i} e_{\dot{\theta}'_i} \tag{22}$$

The calculated torque and thrusts commands will then be sent to each subplane and allocated to the rotor velocities. The physical signals will act on the plant to enable maneuvers according to the internal system dynamics.

C. Stability Analysis

Considering the nominal dynamics, the closed-loop system can be represented in the following format:

$$\begin{aligned}(\dot{e}_R, \dot{e}_\omega) &= f_1(e_R, e_\omega, e_r, \dot{e}_r) \\ (\dot{e}_r, \ddot{e}_r) &= f_2(e_r, \dot{e}_r)\end{aligned} \tag{23}$$

where $e_r = r - r_d$ is the tracking error of the joint position. From the controller design, the first system in (23) is exponentially stable at the origin if $(e_r, \dot{e}_r) = 0$, while the second system in (23) is also exponentially stable. Consequently, we can conclude that the entire system described by (23) is exponentially stable at the origin.

Taking into account the nonlinear terms in the actual system, (23) transforms into:

$$\begin{aligned}&(\dot{e}_R, \dot{e}_\omega) = f_1(e_R, e_\omega, e_r, \dot{e}_r) + \\ &\begin{bmatrix} 0 \\ -M_{res}({}^B\tau_{E,res} - C_{res}) + (M_{res} + \Delta M)^{-1\,B}\tau_{E,res} + \\ (M_{res} + \Delta M)^{-1}(-C_{res} - \Delta C_1 - \Delta C_2) \end{bmatrix} \\ &:= f_1(e_R, e_\omega, e_r, \dot{e}_r) + \begin{bmatrix} 0 \\ \Delta_{f1} \end{bmatrix} \\ &(\dot{e}_r, \ddot{e}_r) = f_2(e_r, \dot{e}_r) + \begin{bmatrix} 0 \\ -\Delta C_3(\omega_0, r, \dot{r}) \end{bmatrix}\end{aligned} \tag{24}$$

where ΔC_1 is composed of the first three rows of $\Sigma_{i=1}^2 J_{iyy} C_{iy}(\beta_i, \dot{\beta}_i, \omega_b)$, ΔC_2 is composed of the first three rows of $\Sigma_{i=1}^2 (J_{ixx} - J_{izz}) C_{ixz}(\beta_i, \dot{\beta}_i, \omega_b)$, and ΔC_3 is composed of the last three rows of $\Sigma_{i=1}^2 (J_{ixx} - J_{izz}) C_{ixz}(\beta_i, \dot{\beta}_i, \omega_b)$. It can be observed that the nonlinear terms C, ΔC_1, ΔC_2, and ΔC_3 can be interpreted as satisfying a linear growth bound: $\|\Delta C_1\| \leq \gamma_1 \|(\omega_0, \dot{r})\|$, $\|\Delta C_2\| \leq \gamma_1 \|(\omega_0, \dot{r})\|$, $\|\Delta C_3\| \leq \gamma_1 \|(\omega_0, \dot{r})\|$, where γ_1, γ_2, and γ_3 are positive constants.

This leads us to the conclusion that the entire closed-loop system described by (24) is exponentially stable in a region containing the origin, if the controller parameters are appropriately selected. It should be noted that the basin of attraction is influenced by the parameters J_y and $J_x - J_z$. The smaller of these two parameters results in a larger γ_1, γ_2 and γ_3, consequently leading to an expanded basin of attraction. This insight can serve as a guiding principle for the structural design criteria of our proposed system.

IV. Simulation Experiment

The proposed control strategy is tested and verified in the Gazebo simulation environment based on the utilities and plugins provided by RotorS, a popular MAV simulator [36].

A. Simulation Setup

1) Model Design: The PADUAV Gazebo model is created by integrating the "Ardrone" model provided by RotorS with a custom frame model defined in URDF (Unified Robot Description Format) syntax, as depicted in Fig. 5. The frame is constructed using five tubes and a center stack, modeled as cylinder basic elements in Gazebo. These elements are properly configured with coordinated and fixed joint relationships. Geometric parameters are chosen to match the subplane size, while other parameters adhere to engineering standards. Key parameters are summarized in Table I.

2) Controller Software Framework: The simulated PADUAV controller software framework is built on the ROS (Robot Operating System) topic communication mechanism, as illustrated in Fig. 6. To replicate real-world communication behavior, four nodes are utilized. The controller node transmits torque and thrust commands to the subplane nodes, which in turn compute motor speeds and relay them to Gazebo. Concurrently, odometry sensors on both the subplanes and the frame provide feedback to update relevant state variables within the PADUAV controller. The framework operates at 100 Hz.

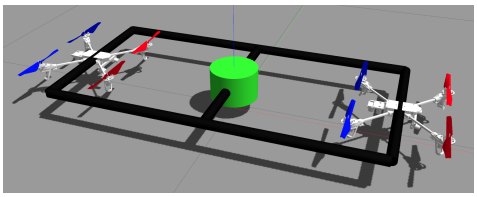

Fig. 5. Gazebo model of PADUAV platform.

TABLE I
PARAMETERS OF THE PADUAV GAZEBO MODEL.

Definition	Symbol	Value in Sim.
Mass of Ardrone	m_i	1.52 kg
Inertia tensor of Ardrone	J_i	0.04, 0.05, 0.10 kg·m^2
Rotor diagonal distance	d_r	0.36 m
Rotor radius	r_{rotor}	0.1 m
Length of the two long tubes	l_{long}	1 m
Length of the three short tubes	l_{short}	0.5 m
Inner radius of the tubes	r_i	0.014 m
Outer radius of the tubes	r_o	0.015 m
Density of the carbon fiber	ρ	1.086×10^3kg/m^3
Height of the center stack	h_c	0.1 m
Radius of the center stack	r_c	0.075 m
Mass of the center stack	m_c	1.3 kg
Mass of the platform	m_b	1.6465 kg

B. Simulation Results

We conducted three experiments to demonstrate the capabilities of the PADUAV platform and its control strategy. These experiments tracked variables denoted as $q =$

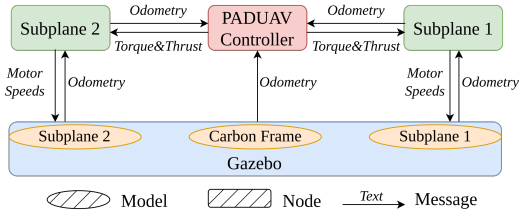

Fig. 6. Controller node communication framework.

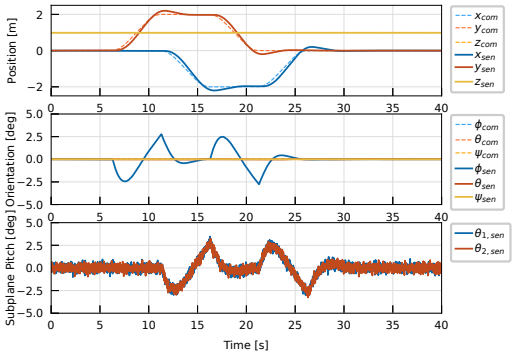

Fig. 7. Rectangular trajectory tracking results. The desired waypoints are $(0, 2, 1)$, $(-2, 2, 1)$, $(-2, 0, 1)$, and $(0, 0, 1)$. The desired pitch and yaw angles are $\psi_d = 0°$ and $\theta_d = 0°$.

$[x, y, z, \psi_b, \theta_b]^T$, representing positions in meters and Euler angles in degrees (with the range between $[-180°, 180°]$). Unless specified otherwise, all trajectories were planned using third-order polynomials, with initial values set to $q_0 = [0, 0, 1, 0, 0]^T$.

1) Rectangular Trajectory Tracking: In this experiment, the platform tracks a rectangular trajectory with each segment lasting 5 seconds. The tracking results in Fig. 7 show that when the PADUAV moves along the y-axis, it exhibits a roll behavior similar to a typical multirotor. However, when the platform moves along the x-axis, it experiences minimal pitch tilt, with more noticeable fluctuations in the subplane pitch angle, demonstrating the translation regulation ability of subplane axial rotation.

2) Continuous Rotation Tracking: This experiment tests the platform's pitch-tracking capability, while other desired values remain the same as the initial settings. The trajectories are depicted in Fig. 8, demonstrating that PADUAV can perform continuous and stable pitch rotations without mechanical limitations or wiring issues, effectively connecting the upper and lower workspaces.

3) Complex Maneuver Tracking: In this experiment, a comprehensive tracking test of all variables is conducted to simulate complex real-life flight tasks. The results, shown in Fig. 9, illustrate successful simultaneous tracking of all five variables. Notably, the z-axis direction transitioned from upward to downward during the flight. This is significant in that it indicates that the PADUAV platform is capable of moving tools installed beneath the platform to the upper workspace. Moreover, the shifting can happen when the platform is tracking position and yaw commands, which increases the autonomy of aerial platforms.

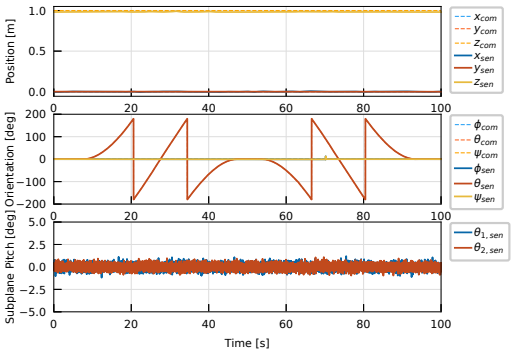

Fig. 8. Continuous rotation tracking results. The platform initially performs a clockwise 720° rotation and, after approximately 10 seconds, executes a counterclockwise 720° rotation.

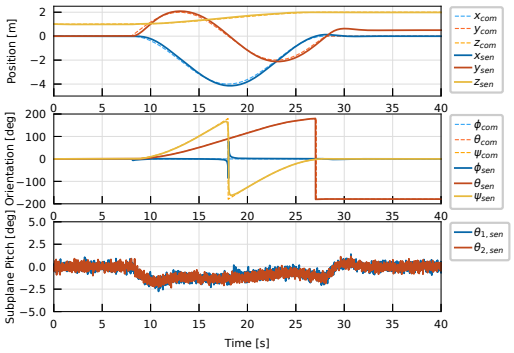

Fig. 9. Complex maneuver tracking results. Over a duration of $T = 20$ s, the platform is expected to execute a circular trajectory with a radius of $r_d = 2$ m in both the x and y directions, described by $x_d(t) = 2\cos(\frac{2\pi}{T}t) - r_d$ and $y_d(t) = 2\sin(\frac{2\pi}{T}t)$, while ascending by 1 m in the z-direction. Additionally, it has to complete a 360° yaw rotation and perform a flip, reaching $\theta_d = 181°$ instead of 180° to avoid repeated jumps in the readout.

V. CONCLUSIONS

In summary, our work introduces the PADUAV, a novel 5-DOF aerial platform designed to overcome traditional tiltrotor limitations. This design eliminates the issues associated with cable winding and opens up new possibilities for tasks like "pick from below and install above" and side valve opening. Also, this paper finds a fresh design perspective for future platforms, that is, the workspace can be conceptually connected and treated as a whole as long as the platform is able to move the installed tools to any orientation. A control framework is developed for PADUAV over its five degrees of freedom. The simulations in the Gazebo environment, utilizing the RotorS simulator, have verified the effectiveness and stability of our control system. Future work includes theoretical handling of singularities, hardware in the loop (HITL) simulation, and real flight tests.

REFERENCES

[1] W. Park, X. Wu, D. Lee, and S. J. Lee, "Design, modeling and control of a top-loading fully-actuated cargo transportation multirotor," 2023.

[2] M. Zhao, K. Nagato, K. Okada, M. Inaba, and M. Nakao, "Forceful valve manipulation with arbitrary direction by articulated aerial robot equipped with thrust vectoring apparatus," *IEEE Robotics and Automation Letters*, vol. 7, no. 2, pp. 4893–4900, 2022.

[3] S. Shimahara, R. Ladig, S. Leewiwatwong, S. Hirai, and K. Shimonomura, "Aerial manipulation for the workspace above the airframe," in *2015 IEEE/RSJ International Conference on Intelligent Robots and Systems (IROS)*, 2015, pp. 1453–1458.

[4] H. Yu, P. Wang, J. Wang, J. Ji, Z. Zheng, J. Tu, G. Lu, J. Meng, M. Zhu, S. Shen *et al.*, "Catch planner: Catching high-speed targets in the flight," *arXiv preprint arXiv:2302.04387*, 2023.

[5] Y. Feng, C. Shi, J. Du, Y. Yu, F. Sun, and Y. Song, "Variable admittance interaction control of uavs via deep reinforcement learning," in *2023 IEEE International Conference on Robotics and Automation (ICRA)*. IEEE, 2023, pp. 1291–1297.

[6] C. Shi, G. Lai, Y. Yu, M. Bellone, and V. Lippiello, "Real-time multi-modal active vision for object detection on uavs equipped with limited field of view lidar and camera," *IEEE Robotics and Automation Letters*, 2023.

[7] Y. Yu and X. Ding, "A global tracking controller for underactuated aerial vehicles: design, analysis, and experimental tests on quadrotor," *IEEE/ASME Transactions on Mechatronics*, vol. 21, no. 5, pp. 2499–2511, 2016.

[8] Zhang, K., Chermprayong, P., Xiao, F. et al. *Aerial additive manufacturing with multiple autonomous robots*. Nature 609, 709–717 (2022).

[9] Sihite, E., Kalantari, A., Nemovi, R. et al. *Multi-Modal Mobility Morphobot (M4) with appendage repurposing for locomotion plasticity enhancement*. Nat Commun 14, 3323 (2023).

[10] F. Ruggiero, V. Lippiello, and A. Ollero, "Aerial manipulation: A literature review," *IEEE Robotics and Automation Letters*, vol. 3, no. 3, pp. 1957–1964, 2018.

[11] D. Sanalitro, M. Tognon, A. J. Cano, J. Cortés, and A. Franchi, "Indirect force control of a cable-suspended aerial multi-robot manipulator," *IEEE Robotics and Automation Letters*, vol. 7, no. 3, pp. 6726–6733, 2022.

[12] T. Lee, "Geometric control of quadrotor uavs transporting a cable-suspended rigid body," *IEEE Transactions on Control Systems Technology*, vol. 26, no. 1, pp. 255–264, 2018.

[13] Y. Yu, C. Shi, D. Shan, V. Lippiello, and Y. Yang, "A hierarchical control scheme for multiple aerial vehicle transportation systems with uncertainties and state/input constraints," *Applied Mathematical Modelling*, vol. 109, pp. 651–678, 2022.

[14] Y. Yu, K. Wang, R. Guo, V. Lippiello, and X. Yi, "A framework to design interaction control of aerial slung load systems: transfer from existing flight control of under-actuated aerial vehicles," *International Journal of Systems Science*, pp. 1–13, 2021.

[15] Y. Yu, R. Guo, K. Wang, and V. Lippiello, "Transfer from existing flight control of under-actuated aerial vehicles to interaction control of aerial slung load systems," in *2021 European Control Conference (ECC)*. IEEE, 2021, pp. 2045–2051.

[16] M. Ryll, D. Bicego, and A. Franchi, "Modeling and control of fast-hex: A fully-actuated by synchronized-tilting hexarotor," in *2016 IEEE/RSJ International Conference on Intelligent Robots and Systems (IROS)*, 2016, pp. 1689–1694.

[17] Y. Yu and Y. Dong, "Global fault-tolerant control of underactuated aerial vehicles with redundant actuators," *International Journal of Aerospace Engineering*, vol. 2019, 2019.

[18] C. Shi and Y. Yu, "Design and implementation of a fully-actuated integrated aerial platform based on geometric model predictive control," *Micromachines*, vol. 13, no. 11, p. 1822, 2022.

[19] J. Sun, Y. Yu, and B. Xu, "Towards flying carpet: Dynamics modeling, and differential-flatness-based control and planning," in *Cognitive Systems and Information Processing: 7th International Conference, ICCSIP 2022, Fuzhou, China, December 17-18, 2022, Revised Selected Papers*. Springer, 2023, pp. 351–370.

[20] Y. Yu and V. Lippiello, "6d pose task trajectory tracking for a class of 3d aerial manipulator from differential flatness," *IEEE Access*, vol. 7, pp. 52 257–52 265, 2019.

[21] C. Shi, Y. Yu, Y. Ma, and D. E. Chang, "Constrained control for systems on matrix lie groups with uncertainties," *International Journal of Robust and Nonlinear Control*, 2022.

[22] R. Ladig, H. Paul, R. Miyazaki, and K. Shimonomura, "Aerial manipulation using multirotor uav: a review from the aspect of operating space and force," *Journal of Robotics and Mechatronics*, vol. 33, no. 2, pp. 196–204, 2021.

[23] M. Kamel, S. Verling, O. Elkhatib, C. Sprecher, P. Wulkop, Z. Taylor, R. Siegwart, and I. Gilitschenski, "The voliro omniorientational hexacopter: An agile and maneuverable tiltable-rotor aerial vehicle," *IEEE Robotics & Automation Magazine*, vol. 25, no. 4, pp. 34–44, 2018.

[24] D. Lee, S. Hwang, C. Kim, S. J. Lee, and H. J. Kim, "Minimally actuated tiltrotor for perching and normal force exertion," 2023.

[25] P. Zheng, X. Tan, B. B. Kocer, E. Yang, and M. Kovac, "Tiltdrone: A fully-actuated tilting quadrotor platform," *IEEE Robotics and Automation Letters*, vol. 5, no. 4, pp. 6845–6852, 2020.

[26] C. Ding and L. Lu, "A tilting-rotor unmanned aerial vehicle for enhanced aerial locomotion and manipulation capabilities: Design, control, and applications," *IEEE/ASME Transactions on Mechatronics*, vol. 26, no. 4, pp. 2237–2248, 2021.

[27] D. Brescianini and R. D'Andrea, "Design, modeling and control of an omni-directional aerial vehicle," in *2016 IEEE International Conference on Robotics and Automation (ICRA)*, 2016, pp. 3261–3266.

[28] S. Park, J. Lee, J. Ahn, M. Kim, J. Her, G.-H. Yang, and D. Lee, "Odar: Aerial manipulation platform enabling omnidirectional wrench generation," *IEEE/ASME Transactions on Mechatronics*, vol. 23, no. 4, pp. 1907–1918, 2018.

[29] H.-N. Nguyen, S. Park, and D. Lee, "Aerial tool operation system using quadrotors as rotating thrust generators," in *2015 IEEE/RSJ International Conference on Intelligent Robots and Systems (IROS)*, 2015, pp. 1285–1291.

[30] H.-N. Nguyen, S. Park, J. Park, and D. Lee, "A novel robotic platform for aerial manipulation using quadrotors as rotating thrust generators," *IEEE Transactions on Robotics*, vol. 34, no. 2, pp. 353–369, 2018.

[31] Y. Su, J. Li, Z. Jiao, M. Wang, C. Chu, H. Li, Y. Zhu, and H. Liu, "Sequential manipulation planning for over-actuated unmanned aerial manipulators," in *International Conference on Intelligent Robots and Systems (IROS)*, 2023.

[32] Y. Su, P. Yu, M. J. Gerber, L. Ruan, and T.-C. Tsao, "Nullspace-based control allocation of overactuated uav platforms," *IEEE Robotics and Automation Letters*, vol. 6, no. 4, pp. 8094–8101, 2021.

[33] P. Yu, Y. Su, M. J. Gerber, L. Ruan, and T.-C. Tsao, "An over-actuated multi-rotor aerial vehicle with unconstrained attitude angles and high thrust efficiencies," *IEEE Robotics and Automation Letters*, vol. 6, no. 4, pp. 6828–6835, 2021.

[34] H. Yang and D. Lee, "Dynamics and control of quadrotor with robotic manipulator," in *2014 IEEE International Conference on Robotics and Automation (ICRA)*, 2014, pp. 5544–5549.

[35] T. Lee, M. Leok, and N. H. McClamroch, "Control of complex maneuvers for a quadrotor uav using geometric methods on se(3)," 2011.

[36] F. Furrer, M. Burri, M. Achtelik, and R. Siegwart, *RotorS—A Modular Gazebo MAV Simulator Framework*. Cham: Springer International Publishing, 2016, pp. 595–625.